RESEARCH ARTICLE   **Open Access**

CrossMark

FTIR microspectroscopy of carbonaceous matter in ~ 3.5 Ga seafloor hydrothermal deposits in the North Pole area, Western Australia

Motoko Igisu[1*] , Yuichiro Ueno[1,2,3] and Ken Takai[1,3]

Abstract

Carbonaceous matter in ~ 3.5 Ga hydrothermal vein deposits from the Dresser Formation, Western Australia, was analyzed using Fourier transform infrared (FTIR) microspectroscopy. Based on the spectroscopy, the carbonaceous matter was mainly composed of disordered aromatic structures, with minor aliphatic C–H functional groups. Spatially resolved analysis supports that the aliphatic C–H signatures are derived from kerogenous macro-molecule and not from free bitumen or other artificial sources. The intensity ratios of the asymmetric aliphatic CH_3 to the asymmetric aliphatic CH_2 ($R_{3/2}$ value) in the carbonaceous clots range from 0.22 to 0.51. Thermal alteration may increase or not change the $R_{3/2}$ value of organic matter, as suggested by previous experiments, but it is unlikely to be the cause of the substantially lower $R_{3/2}$ values when compared with those of primary organic matter. In particular, the low $R_{3/2}$ values ($< \sim 0.4$) suggest that the carbonaceous matter mainly contains aliphatic C–H bonds derived from bacterial cells. The carbonaceous clots may have been possibly produced by abiotic reaction such as Fischer-Tropsch-type (FTT) synthesis. However, the organic matter source only produced by the FTT synthesis is inconsistent with the $R_{3/2}$ values for the analyzed carbonaceous clots. The results obtained by combining these spectroscopic features of the carbonaceous clots together with the previously reported isotopic features may possibly suggest that both bacteria and archaea were colonized in the ~ 3.5 Ga Dresser hydrothermal system.

Keywords: FTIR microspectroscopy, Carbonaceous matter, Dresser formation, Archean

Introduction

Hydrothermal systems have been considered as the origin of life (Holm and Andersson 1998) and the locations of the earliest evolution of life and metabolism (Nisbet 1995). The geological study of ancient hydrothermal systems is crucial to understanding the potential role of hydrothermal systems as the earliest ecosystems. One of Earth's oldest seafloor hydrothermal deposits occurs in the ~ 3.5 Ga Dresser Formation in Western Australia (Fig. 1). In this formation, prominent silica-barite veins containing carbonaceous matter

ubiquitously penetrate pillowed basaltic greenstones (Ueno et al. 2004; Van Kranendonk 2006; Van Kranendonk et al. 2008). The carbonaceous matter in the veins afford an important means of understanding how organic matter was synthesized in the Earth's early hydrothermal systems, although the biological and abiological processes cannot be fully distinguished. The occurrence of biological activity in the Dresser Formation has been inferred from the observation of putative stromatolites (Walter et al. 1980; Van Kranendonk 2006; Van Kranendonk et al. 2008), morphologically preserved putative microfossils (Ueno et al. 2001), microbially induced sedimentary structures (Noffke et al. 2013), and chemical fossils such as ^{13}C-depleted organic matter and methane (Ueno et al. 2001, 2004, 2006) and ^{34}S-depleted pyrites with characteristic $\Delta^{33}S$ (Ueno et al. 2008;
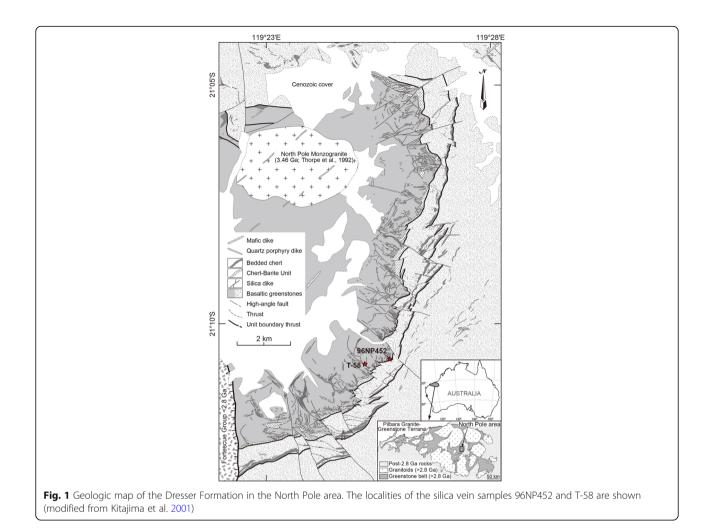
* Correspondence: igisu@jamstec.go.jp
[1]Department of Subsurface Geobiological Analysis and Research, Japan Agency for Marine-Earth Science and Technology (JAMSTEC), 2-15 Natsushima-cho, Yokosuka 237-0061, Japan
Full list of author information is available at the end of the article

Fig. 1 Geologic map of the Dresser Formation in the North Pole area. The localities of the silica vein samples 96NP452 and T-58 are shown (modified from Kitajima et al. 2001)

Shen et al. 2009). Sulfur isotopic signatures also suggest that microbial sulfate reduction was involved in pyrite formation (Ueno et al. 2008; Shen et al. 2009). In addition, ancient hydrothermal fluid inclusions contain ^{13}C-depleted methane, suggesting the presence of methanogenic archaea (Ueno et al. 2006), although it is arguable if those methane were produced by metal-catalyzed abiotic reactions (Sherwood- Lollar and McCollom 2006). The ^{13}C-depletion of organic matter indicates the predominance of autotrophic carbon fixation (Ueno et al. 2001, 2004). The organic matter has been characterized by Raman microspectroscopy, FTIR spectroscopy, solid-state ^{13}C nuclear magnetic resonance, and pyrolysis analysis (e.g., Ueno et al. 2001; Derenne et al. 2008; Duda et al. 2018). The results of these organic geochemical analyses of isolated insoluble organic matter reveal that the organic matter is dominated by aromatic structures with aliphatic hydrocarbon moieties. In addition, the pyrolysis fragments of the organic matter comprise long-chain aliphatic hydrocarbons and thiophenes, which are likely related to the existence of microbes including sulfate-reducing bacteria (Derenne et al. 2008; Duda et al. 2018).

Chemical analyses of Archean organic matter have provided limited but important information about the physiological and phylogenetic characteristics of the source organic compounds (e.g., Hayes 1994; Brocks et al. 1999). Although the observation of morphologically preserved microfossils is a direct evidence of the existence of life, the identification of microfossils based on only morphological analysis is often insufficient (e.g., Brasier et al. 2002; Schopf et al. 2002). The chemical analysis of carbonaceous matter is necessary for understanding its origin and characteristics. However, the bulk analysis of isolated organic matter generally involves the potential risk of post-depositional and experimental contamination of the organic matter (e.g., Brocks et al. 1999; Derenne et al. 2008; Rasmussen et al. 2008; Bourbin et al. 2012). In situ analysis is a more reliable technique that avoids such contamination problems and extracts chemical signatures specific to individual microstructures in petrographic thin sections (e.g., House et al. 2000, 2013; Kudryavtsev et al. 2001; Ueno et al. 2001; Schopf et al. 2002, 2005; Igisu et al. 2006, 2009; van Zuilen et al. 2007; Wacey et al. 2011; Lepot et al. 2013;

Williford et al. 2013). FTIR microspectroscopy has been used to analyze Proterozoic organic-walled acritarchs and bacterial fossils, as well as Phanerozoic miospores (e.g., Arouri et al. 1999, 2000; Marshall et al. 2005; Igisu et al. 2006, 2009; Steemans et al. 2010; Qu et al. 2015). These studies demonstrated the usefulness of IR signatures for characterizing organic-walled microfossils, including those with unknown affinity such as acritarchs. However, FTIR microspectroscopy has not yet been applied to Archean carbonaceous matter in petrographic thin sections. FTIR spectroscopy has been performed on isolated Archean carbonaceous matter, and reported the presence of aliphatic C-H stretching absorptions (Derenne et al. 2008). This previous attempt did not employ the in situ microscopic method. It has been suggested that isolated and powdered samples may be affected by contamination from volatile hydrocarbons in laboratory air (e.g., Salisbury and Walter 1989) and/or from other aliphatic C-H bearing components during sample preparation and storage (e.g., Kebukawa et al. 2009). Therefore, the data from powdered samples would need to be interpreted with caution.

In this paper, we first report the FTIR microspectroscopic features of early Archean carbonaceous matter obtained from two ~ 3.5 Ga silica veins in the Dresser Formation in the North Pole area of Western Australia. The IR signatures are then compared with the characteristics of a variety of biologically and abiotically produced organic compounds, and the possible origins of the carbonaceous clots are discussed.

Methods/Experimental
Samples
We analyzed two samples taken from the silica veins (96NP452 and T-58) that intrude on the basaltic greenstones of the Dresser Formation in the North Pole area of Western Australia. The sampling localities of the silica veins are shown in Fig. 1. Detailed descriptions of the localities and samples can be found in the works of Ueno et al. (2001, 2004, 2006). The Dresser Formation consists of pillowed basaltic greenstones and chert beds. In the North Pole area, these rocks have only undergone low-grade metamorphism below their greenschist facies (Buick and Dunlop 1990; Kitajima et al. 2001; Ueno et al. 2004). The lowest chert unit of the formation is intercalated with several barite beds (Buick and Dunlop 1990), and numerous silica veins intrude the greenstones below the chert/barite beds. The silica veins are 0.3–20 m in width and generally > 100 m in length (Ueno et al. 2001). Zircon U-Pb dating yielded two distinct age groups of 3458 ± 2 Ma (Thorpe et al. 1992a) and 3660 ± 52 Ma (Kitajima et al. 2008) of the felsic unit that overlies the Dresser Formation. A model lead age of 3490 Ma was obtained for galena taken from the Dresser Formation

(Thorpe et al. 1992b), and this may represent the actual depositional age of the formation.

The first doubly polished petrographic thin section sample was made from sample 96NP452 with a thickness of approximately 60 μm. The preparation process was as described by Igisu et al. (2006). We used alumina paste to polish only one side of the thin section to remove interference fringes. To avoid organic contamination during sample preparation, the sample was attached to a glass slide using only a carbon-based dissoluble adhesive (Aron Alpha). The adhesive was used to remove the doubly polished petrographic thin section from the glass slide by immersing in acetone. Petrographic investigation of the thin section indicated that the silica vein sample was mainly composed of microcrystalline quartz (< ~ 10 μm), carbonaceous matter, sulfides, and carbonates (see for example Fig. 2g, h). The filamentous structures described by Ueno et al. (2001) were not observed in the doubly polished thin section.

The second set of doubly polished thin section samples was made from sample T-58 (Ueno et al. 2006) with a thickness of approximately 100 μm. A petrographic examination of the sample revealed three distinctive fabrics, which were denoted by F1–F3 (Fig. 2i). F1 was characterized by coarse-grained quartz (> 1 mm) with abundant fluid inclusions. No carbonaceous matter was observed in F1. F2 comprised microcrystalline quartz chalcedony. Black aggregates in F2 were carbonaceous matter (see Fig. 2i, j) and ion oxides such as hematite. The center of the carbonaceous clot (white part in Fig. 2j) was quartz. F3 consisted mainly of microcrystalline quartz (< ~ 10 μm) and contained carbonaceous matter and ion oxides such as hematite (Fig. 2i). The analyzed carbonaceous clots in the sample were preserved in a microcrystalline quartz matrix or microcrystalline quartz chalcedony, but not in the secondary quartz veins (Fig. 2).
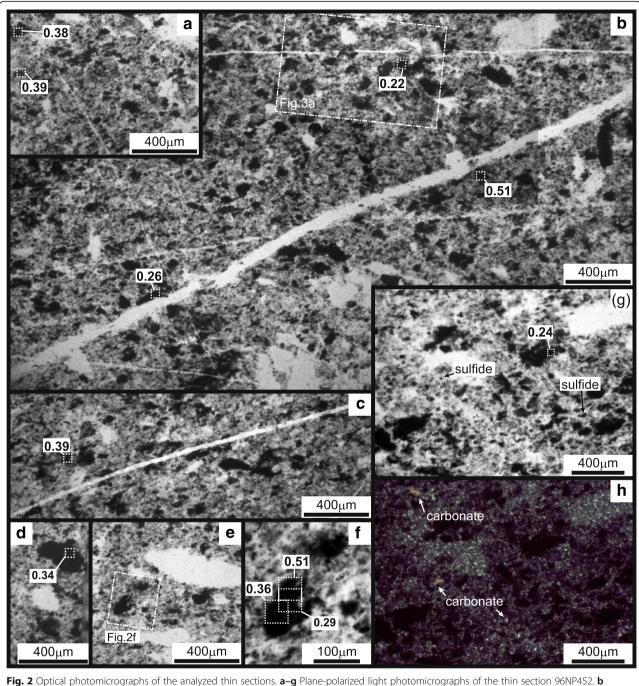
FTIR microspectroscopy
FTIR microspectroscopic analysis was conducted on the two thin section samples using an automated XYZ stage set in an FTIR microspectrometer (JASCO FTIR6200 + IRT7000) with a single-point mercury cadmium telluride detector. The thin section was placed over a hole in the sample holder (Nakashima et al. 1989) and measured as described below.

A reference background spectrum was first measured away from the mounted sample (i.e., in air). A transmission IR spectrum of the sample was then measured. The IR spectrum was described in terms of the IR absorbance, which is a function of the wavenumber (cm^{-1}):
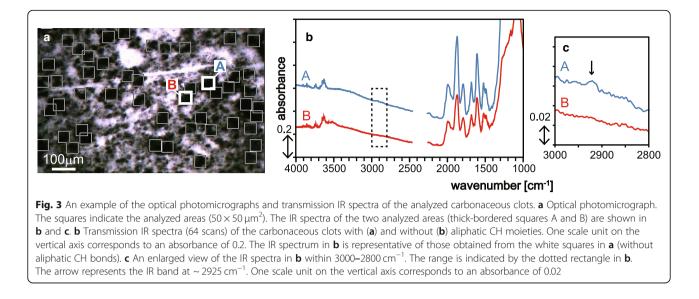
$$\text{Absorbance} = -\log_{10}(T/T_0) \qquad (1)$$

where T and T_0 denote the transmitted intensity of the infrared light at each wavenumber for the sample and air

Fig. 2 Optical photomicrographs of the analyzed thin sections. **a–g** Plane-polarized light photomicrographs of the thin section 96NP452. **b** Composite image of the photomicrographs; the dashed rectangle in **b** corresponds to the area shown in Fig. 3a. **f** Enlarged view of the dashed rectangle in **e**. **h** Cross-polarized light photomicrograph of the same area in **g**. **i, j** Plane-polarized light photomicrographs of the thin section T-58. **i** Composite image of the photomicrographs. **j** Enlarged view of the dashed rectangle in **i**. The locations ($50 \times 50\ \mu m^2$ dotted squares) of the 12 clots with satisfactory signal/noise ratios and their calculated $R_{3/2}$ ratios (1024 scans) are shown in **a–d, f, g, j**

background, respectively. To search for organic signatures, the IR spectra of about 3500 individual carbonaceous clots were first obtained by collecting 64 scans per spot within a spectral range of 4000–1000 cm^{-1} with a 4 cm^{-1} spectral resolution. Among the ~ 3500 examined spots, 47 had an IR absorbance of ~ 2925 cm^{-1}, which indicated excess

analytical error for the adopted 64-scan acquisition mode. These spots were therefore measured again by collecting 1024 scans per spot within a spectral range of 4000–1000 cm^{-1} with a 4 cm^{-1} spectral resolution. This was done to obtain the IR spectra with a better signal-to-noise ratio. Each spectrum was obtained from a spot of $50 \times 50\ \mu m^2$

Fig. 3 An example of the optical photomicrographs and transmission IR spectra of the analyzed carbonaceous clots. **a** Optical photomicrograph. The squares indicate the analyzed areas (50×50 μm^2). The IR spectra of the two analyzed areas (thick-bordered squares A and B) are shown in **b** and **c**. **b** Transmission IR spectra (64 scans) of the carbonaceous clots with (**a**) and without (**b**) aliphatic CH moieties. One scale unit on the vertical axis corresponds to an absorbance of 0.2. The IR spectrum in **b** is representative of those obtained from the white squares in **a** (without aliphatic CH bonds). **c** An enlarged view of the IR spectra in **b** within 3000–2800 cm^{-1}. The range is indicated by the dotted rectangle in **b**. The arrow represents the IR band at ~ 2925 cm^{-1}. One scale unit on the vertical axis corresponds to an absorbance of 0.02

(Figs. 2 and 3a). Duplicate measurements were performed on the 47 spots in the 1024-scan acquisition mode. The analytical errors were determined from the duplicate measurements at the same location as the background spectrum and were found to be smaller than 0.003 absorbance units in the 3000–2800 cm^{-1} range for the 64-scan acquisition mode and smaller than 0.0007 absorbance units for the 1024-scan acquisition mode. All the spectral data were processed using Spectra Manager (JASCO).

Structural characterization of carbonaceous clots
In the aliphatic C–H stretching region (3000–2800 cm^{-1}), the ~ 2925 cm^{-1} band is due to two asymmetric stretching groups, namely, aliphatic CH$_2$ and aromatic CH$_3$ (Jones and Sandorfy 1956; Painter et al. 1981). The band is therefore considered as being the resultant of these two groups. Because the aliphatic CH$_2$ and aromatic CH$_3$ groups have symmetric stretching bands with different peak positions at ~ 2850 and ~ 2870 cm^{-1}, respectively (Bellamy 1954; Jones and Sandorfy 1956), the contribution of the aliphatic CH$_2$ groups can be estimated by elucidating the relationship between the intensities at ~ 2925 cm^{-1} and ~ 2850 cm^{-1}. According to Lambert-Beer's Law:

$$\text{Absorbance} = \varepsilon \cdot c \cdot d, \tag{2}$$

where ε is the molar absorption coefficient, c is the concentration, and d is the sample thickness. Based on Eq. (2), the absorbance ratio between the asymmetric CH$_2$ and symmetric aliphatic CH$_2$ is converted into the ratio of their molar absorption coefficients as follows:

$$\text{Abs}_s/\text{Abs}_a = \varepsilon_s/\varepsilon_a, \tag{3}$$

where Abs$_s$ and Abs$_a$ are respectively the absorbances

(peak heights) of the symmetric aliphatic CH$_2$ and asymmetric aliphatic CH$_2$, and ε_s and ε_a are the corresponding molar absorption coefficients. Thus, if the linear correlation between the peak heights at ~ 2925 and ~ 2850 cm^{-1} is obtained, the ~ 2925 cm^{-1} band would be observed to be mainly due to the aliphatic CH$_2$, and less attributable to the aromatic CH$_3$ group.

The IR signatures of the aliphatic CH$_3$ and CH$_2$ ratios generally reflect the degree of branching and the chain length of the aliphatic hydrocarbon moiety (e.g., Lin and Ritz 1993; Coates 2000). To evaluate the relative length and degree of branching of the aliphatic chain in the carbonaceous clots, we used the aliphatic CH$_3$/CH$_2$ absorbance ratio ($R_{3/2}$):

$$R_{3/2} = \text{Abs}_{CH3}/\text{Abs}_{CH2}, \tag{4}$$

where Abs_{CH3} and Abs_{CH2} respectively denote the peak heights of the asymmetric stretching bands of the aliphatic CH$_3$ (end-methyl, ~ 2960 cm^{-1}) and CH$_2$ (chain-methylene, ~ 2925 cm^{-1}) after linear baseline correction (Igisu et al. 2009). For a more precise determination of $R_{3/2}$, we used only the data for the absorbances at ~ 2960 and 2925 cm^{-1}, which were more than twice the analytical error.

Raman microspectroscopy
A laser Raman micro-spectrometer (Nanophoton RAMANtouch) was used to characterize the carbonaceous clots. Each sample was exposed to a green laser (532 nm wavelength) for a period of 5 s at a laser power density of 1×10^5 W/cm^2. Raman spectra for wavenumbers within ~ 2670–110 cm^{-1} were acquired with a 600 g/mm grating (spectral resolution of ~ 4 cm^{-1}). A × 100 objective lens (NA = 0.9) was used to achieve Raman analysis spatial

Igisu *et al. Progress in Earth and Planetary Science*   (2018) 5:85

Page 6 of 13

resolution of < 1 μm, and the incident laser power was estimated to be ~ 0.4 mW at the sample surface. We only analyzed the carbonaceous matter embedded within the rocks below the surface of the thin section to avoid the effect of polishing, which can induce deformation of carbonaceous matter during sample preparation and thus possibly induce artificial modification of the Raman spectroscopic feature (Pasteris 1989). Prior to sample analyses, wavenumber calibration was determined by comparison with the standard silicon spectra (520 cm^{-1}). All the spectral data were processed using RAMAN viewer (Nanophoton).

Raman spectroscopy has been used as a tool for providing a metamorphic grade indicator of carbonaceous matter in geological samples (e.g., Yui et al. 1996; Beyssac et al. 2002; Rahl et al. 2005; Kouketsu et al., 2014). Several indicators have been proposed to estimate peak metamorphic temperatures by using Raman spectral parameters: peak position, intensity ratio, and full width at half maximum (FWHM) of D band and G band. We chose the D/G band intensity ratio (I_{1350}/I_{1600}) for estimation of the degree of thermal alteration of the carbonaceous matter in order to compare with the previous spectral data of the Proterozoic samples (Qu et al. 2015). The analytical errors for the Raman spectral features were determined by taking duplicate measurements within one area analyzed by FTIR microspectroscopy.

Results and discussion

IR spectra

Figures 3 and 4 show examples of the infrared transmission spectra of the carbonaceous clots in the silica veins. We measured more than 3500 locations in the carbonaceous clots in the thin sections, and only 12 clots had absorbances of ~ 2960, ~ 2925, or ~ 2850 cm^{-1}, which are more than twice the analytical error. The obtained absorbances of ~ 2960, ~ 2925, and ~ 2850 cm^{-1} are summarized in Table 1. The spectrum shown by line B in Fig. 3 was the most common feature in the analyzed carbonaceous clots. This is quite similar to that of the quartz matrix (black line in Fig. 4a, b1, c1), and such data were not used. Instead, some carbonaceous clots show spectral patterns such as A in Fig. 3 (with a peak at ~ 2925 cm^{-1}). The detailed peak assignments of the spectra are explained below.
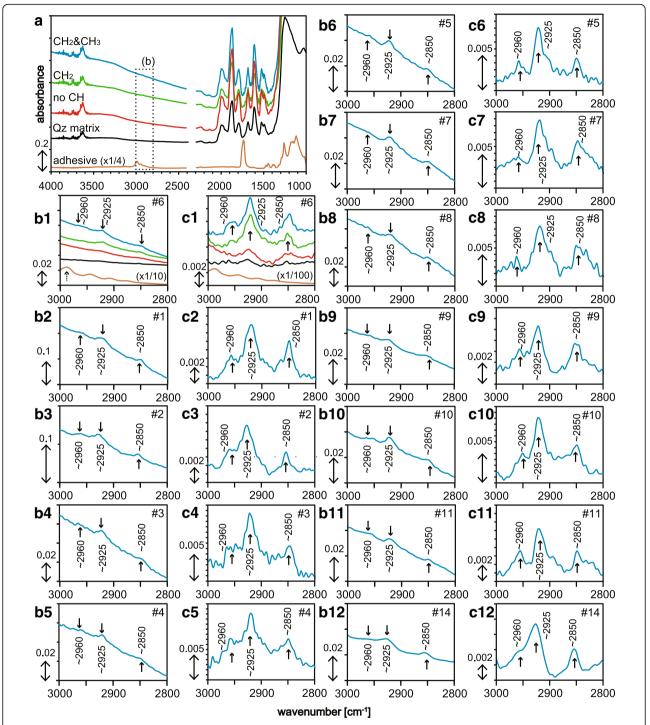
The IR spectrum of the adhesive used to prepare the samples is shown in Fig. 4a, b1, c1. The bands at 2988, 2944, 2908, and 2876 cm^{-1} are due to C–H stretching vibrations. The 1757 cm^{-1} band is due to ester C=O. The 1450 and 1375 cm^{-1} bands are due to C–H bending of $CH_2 + CH_3$ and CH_3 groups, respectively. The bands at 1260 and 1180 cm^{-1} are due to C–N and C–O, respectively. In the 3000–2800 cm^{-1} region, the most intense band for the adhesive is observed at 2988 cm^{-1} (shown by a dotted arrow in Fig. 4b1). Based on the 4 cm^{-1}

wavenumber resolution of the IR spectrometer, the bands of the carbonaceous clots (~ 2960, ~ 2925, and/or ~ 2850 cm^{-1}) are considered to be different from the IR bands of the adhesive. The adhesive used to attach the thin section to the glass has been almost completely washed by acetone. The difference between the absorbances at ~ 2960, ~ 2925, and ~ 2850 cm^{-1} of individual analyzed spots (Table 1) would reflect the amounts of carbonaceous matter and/or its chemical structure. The saturated bands (1400–1000 cm^{-1}) and seven bands (1995, 1870, 1793, 1684, 1610, 1525, and 1492 cm^{-1}) in the figures are due to the Si–O bonds of quartz (Nakashima et al. 1995; Ito and Nakashima 2002; Igisu et al. 2006, 2009; Qu et al. 2015). The IR spectrum around 2300 cm^{-1} is not shown because this range is affected by absorption by CO_2 in the air. In the region of lower wavenumbers of less than 2500 cm^{-1}, the many intense bands of the quartz matrix mask the small signal from the organic matter (Figs. 3 and 4). Hence, we focused on the IR bands with wavenumbers of > 2500 cm^{-1}.

The contribution of the aliphatic CH_2 group to the intensity in the ~ 2925 cm^{-1} band was examined by comparison with those in the ~ 2925 and ~ 2850 cm^{-1} band. Figure 5 shows the relationship between the intensities in the ~ 2925 and ~ 2850 cm^{-1} bands. The strong correlation between these two bands suggests that they are due to the same component(s) and that the ~ 2925 cm^{-1} band of the carbonaceous clots is mostly due to the aliphatic CH_2 and is less attributable to the aromatic CH_3 groups. These results indicate that the Dresser carbonaceous clots contain small amounts of aliphatics.

Raman spectral data

The carbonaceous clots in sample 96NP452 have disordered carbonaceous structures, which were observed as ~ 1600 cm^{-1} (graphite, G) and ~ 1350 cm^{-1} (disordered, D) bands in the Raman spectra (Fig. 6). Their Raman spectral features are shown in Table 1 and are similar to each other for this sample. They are also consistent with the previously reported data (Ueno et al. 2001, 2004) and those of carbonaceous matter from lower greenschist facies metasediments (Yui et al. 1996). In addition, it is inconsistent with the carbonaceous matter with different thermal alteration phases observed in ~ 3.46 Ga hydrothermal Apex Chert (Olcott-Marshall et al. 2012; Sforna et al. 2014). These Raman and IR spectral features of the carbonaceous clots suggest that the clots mainly consist of randomly arranged layered polyaromatic domains with minor aliphatic C–H bonds. On the other hand, the carbonaceous clot in sample T-58 does not show clear G or D bands. Instead, it shows a sloping baseline (Fig. 6), possibly suggesting fluorescence produced by hydrogen-rich saturated aliphatic hydrocarbons (Marshall et al. 2005). However, this appears inconsistent

Fig. 4 The transmission IR absorbance spectra (1024 scans) of the carbonaceous clots. **a** Examples of the IR spectra of the carbonaceous clots with aliphatic CH$_2$ and CH$_3$ bonds (blue line: spot #6 in Table 1), only aliphatic CH$_2$ bond (green line: spot #12 in Table 1), and no CH$_2$ bond (red line: spot #13 in Table 1) together with quartz matrix (black line). IR transmission-reflection spectrum of the carbon-based dissolvable adhesive used in this study on an aluminum foil is shown by the brown line (modified from Igisu et al. 2006). One scale unit on the vertical axis corresponds to an absorbance of 0.2. (b) An enlarged view of the IR spectra within 3000–2800 cm^{-1}. The range for **b1** is indicated by the dotted rectangle in **a**. Spot numbers (#1, #2, etc.) are shown in the upper right in each figure. One scale unit on the vertical axis corresponds to an absorbance of 0.02 in **b1** and **b4**–**b12**, and 0.1 in **b2** and **b3**. **c** The IR spectra after linear baseline correction of the spectra in **b** within 3000–2800 cm^{-1}. Spot numbers (#1, #2, etc.) are shown in the upper right in each figure. One scale unit on the vertical axis corresponds to an absorbance of 0.002 in **c1** and **c12**, and 0.001 in **c2**–**c11**. The spectra of the adhesive are re-scaled to a quarter in **a**, one-tenth in **b1**, and one-hundredth in **c1** for clarity

Table 1 IR and Raman parameters for analyzed carbonaceous clots

Sample #	Spot #	Microphotograph	IR				Raman				
			Abs at ~ 2960 cm^{-1}	Abs at ~ 2925 cm^{-1}	Abs at ~ 2850 cm^{-1}	$R_{3/2}$	I_{1350}/I_{1600}	A_{1350}/A_{1600}	$FWHM_{1350}$	$FWHM_{1600}$	N
96NP452	#1	Figure 2a	0.0024 ± 0.0003	0.0062 ± 0.0005	0.0043 ± 0.0000	0.38 ± 0.02	1.54 ± 0.07	2.21 ± 0.06	65.0 ± 4.9	45.1 ± 3.0	27
	#2	Figure 2a	0.0019 ± 0.0001	0.0050 ± 0.0002	0.0018 ± 0.0001	0.39 ± 0.00	1.46 ± 0.07	2.24 ± 0.07	67.6 ± 4.3	44.2 ± 2.9	28
	#3	Figure 2b	0.0025 ± 0.0000	0.0088 ± 0.0010	0.0046 ± 0.0007	0.29 ± 0.03	1.45 ± 0.08	2.24 ± 0.05	68.3 ± 5.1	44.2 ± 2.2	27
	#4	Figure 2b	0.0051 ± 0.0003	0.0100 ± 0.0005	0.0055 ± 0.0000	0.51 ± 0.01	1.46 ± 0.06	2.23 ± 0.03	67.1 ± 2.9	43.8 ± 1.3	27
	#5	Figure 2b	0.0025 ± 0.0001	0.0070 ± 0.0006	0.0039 ± 0.0008	0.36 ± 0.05	1.52 ± 0.08	2.22 ± 0.08	63.2 ± 4.3	43.2 ± 3.1	27
	#6	Figure 2c	0.0017 ± 0.0000	0.0052 ± 0.0001	0.0026 ± 0.0001	0.34 ± 0.01	1.39 ± 0.07	2.20 ± 0.08	70.8 ± 5.5	44.8 ± 3.0	27
	#7	Figure 2d	0.0016 ± 0.0004	0.0066 ± 0.0005	0.0034 ± 0.0004	0.24 ± 0.04	1.47 ± 0.08	2.24 ± 0.04	65.1 ± 3.1	42.6 ± 1.2	27
	#8	Figure 2f	0.0018 ± 0.0005	0.0073 ± 0.0009	0.0040 ± 0.0005	0.26 ± 0.10	1.48 ± 0.06	2.25 ± 0.06	66.3 ± 2.7	43.6 ± 2.2	30*
	#9	Figure 2f	0.0014 ± 0.0001	0.0038 ± 0.0001	0.0024 ± 0.0000	0.39 ± 0.05	1.48 ± 0.06	2.25 ± 0.06	66.3 ± 2.7	43.6 ± 2.2	30*
	#10	Figure 2f	0.0021 ± 0.0003	0.0094 ± 0.0001	0.0048 ± 0.0002	0.22 ± 0.03	1.46 ± 0.04	2.26 ± 0.04	66.7 ± 1.6	42.9 ± 0.9	30
	#11	Figure 2g	0.0026 ± 0.0002	0.0050 ± 0.0003	0.0024 ± 0.0002	0.51 ± 0.00	1.49 ± 0.08	2.25 ± 0.03	65.8 ± 3.9	43.4 ± 1.4	28
	#12		n.d.	0.0042 ± 0.0001	0.0015 ± 0.0002		1.40 ± 0.06	2.24 ± 0.03	69.6 ± 2.5	43.6 ± 0.9	27
	#13		n.d.	n.d.	n.d.		1.36 ± 0.13	2.00 ± 0.37	77.9 ± 8.8	52.4 ± 12.7	27
T-58	#14	Figure 2j	0.0021 ± 0.0000	0.0056 ± 0.0004	0.0025 ± 0.0001	0.38 ± 0.02					

Absorbances at ~ 2960 cm^{-1}, ~ 2925 cm^{-1}, and 2850 cm^{-1} and $R_{3/2}$ values of the analyzed carbonaceous matter. Errors show standard deviations. *n.d.* not detected
*The same data are shown because the analyzed area for FTIR microspectroscopy of the clots were overlapped

with the IR data that the absorbance of aliphatic CH_2 in the carbonaceous clots in sample T-58 falls within the range for those in sample 96NP452 (Fig. 5). The inconsistency between the Raman and IR data of the carbonaceous clots in sample T-58 and sample 96NP452 may be due to difference in the amounts of organic matter. Raman spectral data suggest that the analyzed carbonaceous clots at least in sample 96NP452 are moderately graphitized by metamorphism, supporting indigenous origin in ca. 3.5 Ga rocks rather than contaminations.

Spatial distributions of aliphatic C–H groups

The $R_{3/2}$ values of the carbonaceous clots range from 0.22 ± 0.03 to 0.51 ± 0.01 (Fig. 7 and Table 1). In sample 96NP452, some of the carbonaceous clots containing aliphatic C–H signatures were located relatively close (< 100 μm) to the secondary quartz veins (Fig. 2b, c), while others were far (> 100 μm) from the veins (Fig. 2e, g). Both low (~ 0.3) and high (~ 0.5) $R_{3/2}$ values were observed within one carbonaceous clot (Fig. 2f) and also

along one secondary quartz vein (Fig. 2b). In sample T-58, one carbonaceous clot with aliphatic C–H signatures was observed in the quartz chalcedony (F2; Fig. 2i), while the other carbonaceous clots in the quartz chalcedony and microcrystalline quartz did not have aliphatic C–H signatures. These results indicate the absence of an apparent distribution pattern among the carbonaceous clots with and without aliphatic C–H signatures. In addition, there was significant variation among the $R_{3/2}$ values within a given sample, and even within a given carbonaceous clot. The aliphatic C–H signatures of the carbonaceous clots are spatially heterogeneous on a micrometer to millimeter scale.

Origin of the carbonaceous matter

Post-depositional thermal alteration of the primary organic matter may have altered the $R_{3/2}$ values. The varying $R_{3/2}$ values of the carbonaceous clots may also be explained by a mixture of different sources of biological organic compounds and/or abiotically

Fig. 5 Relationship between the intensities of the carbonaceous clots at ~ 2925 cm^{-1} and ~ 2850 cm^{-1}. The ~ 2925 cm^{-1} band is due to asymmetric stretching vibrations of the aliphatic CH$_2$ and aromatic CH$_3$, and the ~ 2850 cm^{-1} band is due to symmetric stretching vibration of the aliphatic CH$_2$. The yellow diamonds indicate the data for sample 96NP452, while the green diamond indicates that for sample T-58. The error bars indicate the standard deviations of the duplicate measurements

produced compounds. The possible occurrence of anaerobic chemoautotrophic microorganisms was suggested by the carbon isotopic signatures of the carbonaceous matter in the silica veins in the Dresser Formation (Ueno et al. 2004). The carbon isotopic signatures provide the potential chemical evidence of microbial activity in the environment at the time, but do not
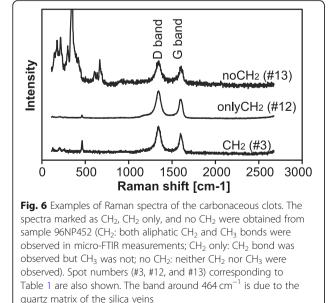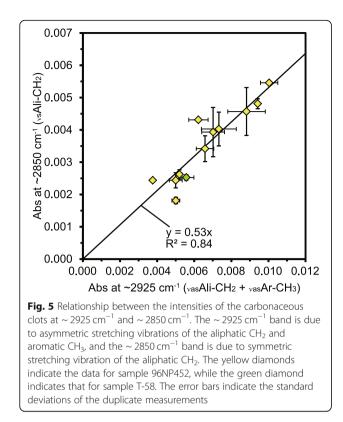

Fig. 6 Examples of Raman spectra of the carbonaceous clots. The spectra marked as CH$_2$, CH$_2$ only, and no CH$_2$ were obtained from sample 96NP452 (CH$_2$: both aliphatic CH$_2$ and CH$_3$ bonds were observed in micro-FTIR measurements; CH$_2$ only: CH$_2$ bond was observed but CH$_3$ was not; no CH$_2$: neither CH$_2$ nor CH$_3$ were observed). Spot numbers (#3, #12, and #13) corresponding to Table 1 are also shown. The band around 464 cm^{-1} is due to the quartz matrix of the silica veins
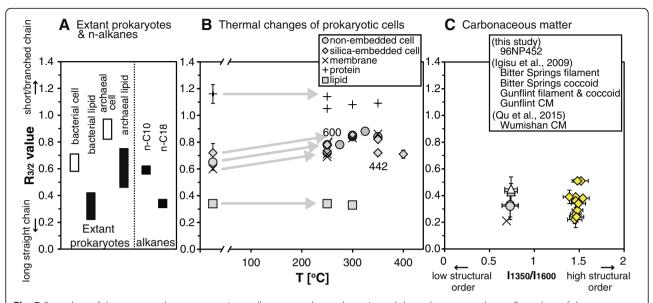
necessarily offer clues for distinguishing whether the products are derived from the microbial functions of the bacterial and/or the archaeal populations. The existence of sulfate-reducing bacteria has been proposed by the pyrolysis fragments of the organic matter (Derenne et al. 2008). However, the potential risk of post-depositional and experimental contamination has been found in the pyrolysis analysis of the isolated Archean organic matter (e.g., Bourbin et al. 2012). The presence of ancient methanogenic archaea has been inferred from the fluid inclusions in the silica veins containing ^{13}C-depleted methane (Ueno et al. 2006), although the abiotic origin of the methane has also been proposed (Sherwood-Lollar and McCollom 2006). We will discuss the origin of the varying $R_{3/2}$ values for the carbonaceous clots in the following order: (1) abiological origin, (2) effect of thermal alteration, and (3) biological origin.

Abiological origin

It is known that an FTT synthesis under specific hydrothermal conditions (e.g., in ultramafic rock-associated hydrothermal systems) may produce organic compounds (e.g., Yanagawa and Kobayashi 1992; Holm and Andersson 1998; McCollom et al. 1999; McCollom and Seewald 2006). The organic products of the FTT synthesis are mainly methane and normal alkanes with only a small amount of branched hydrocarbons because the relative abundance of these hydrocarbons decreases with increasing carbon number in the alkyl chains (McCollom and Seewald 2006, 2007). McCollom and Seewald (2006) reported that isobutane was the only branched product of FTT synthesis, but the yield of isobutane (~ 0.02 mmol/kg) was much lower than those of the normal alkanes (e.g., 0.64 mmol/kg for n-butane). Therefore, it is supposed that mixing of the organic matter produced by the synthesis (mainly the short-chain products) increases the $R_{3/2}$ value. Although we did not directly determine the carbon number of the aliphatic components in the carbonaceous clots, the $R_{3/2}$ values for the normal C$_{10}$ alkane are estimated to be ~ 0.6 (Fig. 7a; data from Igisu et al. 2009). The relative abundance of the saturated > C$_{10}$ hydrocarbons produced by the FTT synthesis has been shown to be several orders of magnitude lower than those of the saturated < C$_6$ hydrocarbons (McCollom and Seewald 2006). Thus, it appears to be difficult to explain the observed $R_{3/2}$ values of the carbonaceous clots (0.22–0.51) at this stage based solely on abiotically produced organic matter. Moreover, it is unlikely that the FTT synthesis of organic compounds occurs during the formation of the silica veins. This is because native Fe–Ni minerals and other preferred catalysts for FTT reactions were not observed in the thin sections of the present study.

Fig. 7 $R_{3/2}$ values of the extant prokaryotes, experimentally maturated cyanobacteria, and the carbonaceous clots. **a** $R_{3/2}$ values of the extant bacterial and archaeal cells and lipids (data from Igisu et al. 2012) together with the standard n-alkane samples (n-C$_{10}$ and n-C$_{18}$) (data from Igisu et al. 2009). The $R_{3/2}$ values for the representative extant untreated bacterial and archaeal cells range from 0.59 ± 0.01 to 0.70 ± 0.01 and from 0.86 ± 0.04 to 0.95 ± 0.02, and those for bacterial and archaeal lipids range from 0.31 ± 0.09 to 0.41 ± 0.01 and from 0.51 ± 0.05 to 0.67 ± 0.08, respectively. **b** Results of the heating experiments for the non-embedded and silica-embedded cyanobacterial cells (modified from Igisu et al. 2009, 2018). The $R_{3/2}$ values for the heated samples are plotted against the heating temperature. All the experimental run products of the silica-embedded samples were obtained after heating for 600 min except the one indicated by a number (the sample marked was heated for 442 min). Others were obtained after heating for 300 min except the one indicated by a number (the sample marked was heated for 600 min). **c** $R_{3/2}$ values of the carbonaceous clots obtained from the Dresser Formation together with the Proterozoic prokaryotic fossils and carbonaceous matter (CM) in stromatolite. The error bars for the carbonaceous clots indicate the standard deviations of the duplicate measurements. The data for Bitter Springs and Gunflint samples were obtained from Igisu et al. (2009), and that for Wumishan sample was obtained from Qu et al. (2015)

Effect of thermal alteration

Thermal alteration may increase or not change the $R_{3/2}$ value of organic matter. This indicates the preferential loss of the methylene group and/or formation of branched CH$_3$ in the aliphatic structures during the degradation of the organic matter, as revealed by FTIR measurements of coal (Wang and Griffiths 1985; Ibarra et al. 1996), and heating experiments performed on kerogens (Robin et al. 1977; Huang and Otten 1998) and extant cyanobacteria (Igisu et al. 2009, 2018). Recently, a kinetic approach applied to experimental maturation of cyanobacteria revealed that decreasing rate constants for aliphatic CH$_3$ were generally similar to or lower than aliphatic CH$_2$ at 250–450 °C under both non-embedded and silica-embedded conditions. This suggests that aliphatic CH$_3$ groups degraded more slowly than aliphatic CH$_2$ groups (Igisu et al. 2018). The metamorphic grade of basaltic greenstones surrounding the silica veins is generally below the greenschist facies (< 350 °C; Kitajima et al. 2001). Thermal alteration may therefore explain the varying $R_{3/2}$ values, but is unlikely to be the cause of the substantially lower $R_{3/2}$ values when compared with those of primary organic matter.

In addition, the coexistence of carbonaceous matter with different degrees of thermal alteration may cause variation in the $R_{3/2}$ value and the presence/absence of aliphatic C–H signatures in the carbonaceous clots. There is the possibility of contribution of some molecules and/or some functional groups, which are very resistant to heat even if they suffered from the same heating processes, to the carbonaceous clots. Assuming that some parts of the molecules and groups were graphitized but some parts were not, there may be differences in the $R_{3/2}$ values and Raman spectral features observed in the carbonaceous clots in samples 96NP452 and T-58. Such heterogeneity was reported in Phanerozoic eukaryotic fossils (Qu et al. 2015).

Biological origin

The $R_{3/2}$ values for the carbonaceous clots in the present study (0.22–0.51) generally fall within the range for extant bacterial and archaeal cellular compounds (Fig. 7a, c). The observed low $R_{3/2}$ values below ~ 0.4 cannot be explained by the degraded cellular compounds other than degraded bacterial lipids, possibly representing the relatively bacteria-dominated fractions of the microbial communities. On the other hand, there are carbonaceous clots with higher $R_{3/2}$ values (> ~ 0.4). Such carbonaceous clots may be caused by thermal alteration of organic matter with lower $R_{3/2}$ values or be derived from the archaea-dominated assemblages as well as

compounds with short-chain aliphatic components. Such a possible contribution of aliphatic components to geo-macromolecules by living organisms without resistant aliphatic precursors (e.g., algaenan) has been suggested by Gupta et al. (2007a, 2007b, 2014).

A comparison of the $R_{3/2}$ values of the carbonaceous clots with those of other Proterozoic prokaryotic fossils and carbonaceous matter in the stromatolites (~ 830 Ma Bitter Springs Group, ~ 1500 Ma Wumishan Group, and ~ 1900 Ma Gunflint Formation) reveals that the carbonaceous clots have similar $R_{3/2}$ values as other Proterozoic samples (Fig. 7c), while the Raman spectra of the carbonaceous clots show a more graphitized nature than those of the Proterozoic microfossils (i.e., narrower bandwidth of especially the D band and higher D/G band intensity ratio). This suggests the possible interpretation of the prokaryotic origin of the carbonaceous clots, assuming that the $R_{3/2}$ value either increases or remains unchanged during the thermal degradation processes.

Given that the aliphatic moieties in the carbonaceous clots might indicate the presence of cellular organic aggregates of the prokaryotic population in the ancient microbial communities, the IR spectroscopic features of the carbonaceous clots likely suggest a contribution from the bacterial lipids in the ancient microbial communities associated with the hydrothermal activities. Our results thus afford additional important insights into the indigenous microbial communities in the ~ 3.5 Ga Dresser seafloor hydrothermal system that consists of not only archaeal components, but also significant bacterial populations. This supports the previous pyrolysis analysis of the isolated organic matter, suggesting microbial origin of the organic matter (Derenne et al. 2008; Duda et al. 2018).

Conclusions

FTIR microspectroscopic analysis was conducted on carbonaceous clots taken from two silica veins in the ~ 3.5 Ga Dresser Formation. We found the following:

1. The chemical structure of the carbonaceous clots comprises randomly arranged layered polyaromatic domains with very minor aliphatic straight chain moieties.
2. It appears unlikely at this stage that the observed $R_{3/2}$ values of the carbonaceous clots and the mineral assemblages in the analyzed samples do not support the only abiogenic origin of the carbonaceous clots.
3. Thermal alteration may increase or not change the $R_{3/2}$ value of organic matter. Therefore, it may explain the varying $R_{3/2}$ values, but is unlikely to be the cause of the substantially lower $R_{3/2}$ values

when compared with those of primary organic matter.
4. The $R_{3/2}$ values of the carbonaceous clots (0.22–0.51) generally fall within the range of the values for extant prokaryotic cellular components. In particular, the low $R_{3/2}$ values ($< \sim 0.4$) could have originated from bacterial lipid, assuming that the $R_{3/2}$ value would either increase or remain unchanged during the thermal degradation processes. This suggests the preservation of remnants of the bacterial population, mainly as aliphatic C–H groups, in the macromolecular structure of the analyzed carbonaceous matter.

The new FTIR microspectroscopic data of the carbonaceous clots combined with the previous studies based on their isotopic features (e.g., Ueno et al. 2001, 2004, 2006) may possibly suggest that both bacteria and archaea were colonized in the ~ 3.5 Ga Dresser hydrothermal system.

Availability of data and materials
Please contact the corresponding author regarding data requests.

Authors' contributions
MI and YU proposed and designed the study. YU conducted the fieldwork and sampling. MI carried out the measurements, analyzed the data, and drafted the manuscript. YU and KT collaborated with the corresponding author in the interpretation of the data and the construction of the manuscript. All authors read and approved the final manuscript.

Competing interests
The authors declare that they have no competing interests.

Publisher's Note
Springer Nature remains neutral with regard to jurisdictional claims in published maps and institutional affiliations.

Author details
[1]Department of Subsurface Geobiological Analysis and Research, Japan Agency for Marine-Earth Science and Technology (JAMSTEC), 2-15 Natsushima-cho, Yokosuka 237-0061, Japan. [2]Department of Earth and Planetary Sciences, Tokyo Institute of Technology, 2-12-1 O-okayama, Meguro-ku, Tokyo 152-8551, Japan. [3]Earth-Life Science Institute, Tokyo Institute of Technology, 2-12-1 O-okayama, Meguro-ku, Tokyo 152-8551, Japan.

References

Arouri K, Greenwood PF, Walter MR (1999) A possible chlorophycean affinity of some Neoproterozoic acritarchs. Org Geochem 30:1323–1337

Arouri K, Greenwood PF, Walter MR (2000) Biological affinities of Neoproterozoic acritarchs from Australia: microscopic and chemical characterisation. Org Geochem 31:75–89

Bellamy LJ (1954) The infra-red spectra of complex molecules. John Wiley & Sons, New York

Beyssac O, Goffé B, Chopin C, Rouzaud JN (2002) Raman spectra of carbonaceous material in metasediments: a new geothermometer. J Metamorph Geol 20:859–871

Bourbin M, Derenne S, Robert F (2012) Limits in pyrolysis-GC-MS analysis of kerogen isolated from Archean cherts. Org Geochem 52:32–34

Brasier MD, Green OR, Jephcoat AP, Kleppe AK, Van Kranendonk MJ, Lindsay JF, Steele A, Grassineau NV (2002) Questioning the evidence for Earth's oldest fossils. Nature 416:76–81

Brocks JJ, Logan GA, Buick R, Summons RE (1999) Archean molecular fossils and the early rise of eukaryotes. Science 285:1033–1036

Buick R, Dunlop JSR (1990) Evaporitic sediments of early Archean age from the Warrawoona Group, North Pole, Western Australia. Sedimentology 37:247–277

Coates J (2000) Interpretation of infrared spectra, a practical approach. In: Meyers RA (ed) Encyclopedia of analytical chemistry. John Wiley & Sons Ltd, UK

Derenne S, Robert F, Skrzypczak-Bonduelle A (2008) Molecular evidence for life in the 3.5 billion year old Warrawoona chert. Earth Planet Sci Lett 272:476–480

Duda JP, Thiel V, Bauersachs T, Mißbach H, Reinhardt M, Schäfer N, Van Kranendonk MJ, Reitner J (2018) Ideas and perspectives: hydrothermally driven redistribution and sequestration of early Archaean biomass—the "hydrothermal pump hypothesis". Biogeosciences 15:1535–1548

Gupta NS, Briggs DEG, Collison ME, Evershed RP, Michels R, Jack KS, Pancost RD (2007b) Evidence for the in situ polymerization of labile aliphatic organic compounds during the preservation of fossil leaves: implications for organic matter preservation. Org Geochem 38:499–522

Gupta NS, Michels R, Briggs DEG, Collison ME, Evershed RP, Pancost RD (2007a) Experimental evidence for the formation of geomacromolecules from plant leaf lipids. Org Geochem 38:28–36

Gupta NS, Steele A, Fogel M, Griffin P, Adams M, Summons RE, Yang H, Cody GD (2014) Experimental formation of geomacromolecules from microbial lipids. Org Geochem 67:35–40

Hayes JM (1994) Global methanotrophy at the Archaean-Proterozoic transition. In: Bengtson S (ed) Early life on earth. Columbia University Press, New York

Holm NG, Andersson EM (1998) Hydrothermal systems. In: Brack A (ed) The molecular origins of life. Cambridge University Press, Cambridge

House CH, Oehler DZ, Sugitani K, Mimura K (2013) Carbon isotopic analyses of ca. 3.0 Ga microstructures imply planktonic autotrophs inhabited Earth's early oceans. Geology 41:651–654

House CH, Schopf JW, McKeegan KD, Coath CD, Harrison TM, Stetter KO (2000) Carbon isotopic composition of individual Precambrian microfossils. Geology 28:707–710

Huang WL, Otten GA (1998) Oil generation kinetics determined by DAC-FS/IR pyrolysis: technique development and preliminary results. Org Geochem 29:1119–1137

Ibarra JV, Muñoz E, Moliner R (1996) FTIR study of the evolution of coal structure during the coalification process. Org Geochem 24:725–735

Igisu M, Nakashima S, Ueno Y, Awramik SM, Maruyama S (2006) In situ infrared microspectroscopy of ~850 million-year-old prokaryotic fossils. Appl Spectrosc 60:1111–1120

Igisu M, Takai K, Ueno Y, Nishizawa M, Nunoura T, Hirai M, Kaneko M, Naraoka H, Shimojima M, Hori K, Nakashima S, Ohta H, Maruyama S, Isozaki Y (2012) Domain-level identification and quantification of relative prokaryotic cell abundance in microbial communities by micro-FTIR spectroscopy. Environ Microbiol Rep 4:42–49

Igisu M, Ueno Y, Shimojima M, Nakashima S, Awramik SM, Ohta H, Maruyama S (2009) Micro-FTIR signature of bacterial lipids in Proterozoic microfossils. Precambrian Res 173:19–26

Igisu M, Yokoyama T, Ueno Y, Nakashima S, Shimojima M, Ohta H, Maruyama S (2018) Changes of aliphatic C–H bonds in cyanobacteria during experimental thermal maturation in the presence or absence of silica as evaluated by FTIR microspectroscopy. Geobiology 16:412–428

Ito Y, Nakashima S (2002) Water distribution in low-grade siliceous metamorphic rocks by micro-FTIR and its relation to grain size: a case from the Kanto Mountain region, Japan. Chem Geol 189:1–18

Jones RN, Sandorfy C (1956) The application of infrared and Raman spectrometry to the elucidation of molecular structure. In: Weissberger A (ed) Technique of organic chemistry Vol. IX. Interscience Publishers, New York

Kebukawa Y, Nakashima S, Otsuka T, Nakamura-Messenger K, Zolensky ME (2009) Rapid contamination during storage of carbonaceous chondrites prepared for micro FTIR measurements. Meteorit Planet Sci 44:545–557

Kitajima K, Hirata T, Maruyama S, Yamanashi T, Sano Y, Liou JG (2008) U-Pb zircon geochronology using LA-ICP-MS in the North Pole Dome, Pilbara craton, Western Australia: a new tectonic growth model for the Archean chert/greenstone succession. Int Geol Rev 50:1–14

Kitajima K, Maruyama S, Utsunomiya S, Liou JG (2001) Seafloor hydrothermal alteration at an Archaean mid-ocean ridge. J Metamorph Geol 19:583–599

Kouketsu Y, Mizukami T, Mori H, Endo S, Aoya M, Hara H, Nakamura D, Wallis S (2014) A new approach to develop the Raman carbonaceous material geothermometer for low-grade metamorphism using peak width. Island Arc 23:33–50

Kudryavtsev AB, Schopf JW, Agresti DG, Wdowiak TJ (2001) In situ laser-Raman imagery of Precambrian microscopic fossils. Proc Natl Acad Sci 98:823–826

Lepot K, Williford KH, Ushikubo T, Sugitani K, Mimura K, Spicuzza MJ, Valley JW (2013) Texture-specific isotopic compositions in 3.4 Gyr old organic matter support selective preservation in cell-like structures. Geochim Cosmochim Acta 112:66–86

Lin R, Ritz GP (1993) Reflectance FT-IR microspectroscopy of fossil algae contained in organic-rich shales. Appl Spectrosc 47:265–271

Marshall CP, Javaux EJ, Knoll AH, Walter MR (2005) Combined micro-Fourier transform infrared (FTIR) spectroscopy and micro-Raman spectroscopy of Proterozoic acritarchs: a new approach to palaeobiology. Precambrian Res 138:208–224

McCollom TM, Ritter G, Simoneit BRT (1999) Lipid synthesis under hydrothermal conditions by Fischer-Tropsch-type reactions. Origins of Life and Evolution of Biospheres 29:153–166

McCollom TM, Seewald JS (2006) Carbon isotope composition of organic compounds produced by abiotic synthesis under hydrothermal conditions. Earth Planet Sci Lett 243:74–84

McCollom TM, Seewald JS (2007) Abiotic synthesis of organic compounds in deep-sea hydrothermal environments. Chem Rev 107:382–401

Nakashima S, Matayoshi H, Yuko T, Michibayashi K, Masuda T, Kuroki N, Yamagishi H, Ito Y, Nakamura A (1995) Infrared microspectroscopy analysis of water distribution in deformed and metamorphosed rocks. Tectonophysics 245:263–276

Nakashima S, Ohki S, Ochiai S (1989) Infrared microspectroscopy analysis of the chemical state and spatial distribution of hydrous species in minerals. Geochem J 23:57–64

Nisbet EG (1995) Archaean ecology: a review of evidence for the early development of bacterial biomes and speculations on the development of a global-scale biosphere. In: Coward MP, Ries AC (eds) Early Precambrian processes. Geological Society Special Publication, London

Noffke N, Christian D, Wacey D, Hazen RP (2013) Microbially induced sedimentary structures recording an ancient ecosystem in the ca. 3.48 billion-year-old Dresser Formation, Pilbara, Western Australia. Astrobiology 13:1103–1124

Olcott-Marshall A, Emry JR, Marshall CP (2012) Multiple generations of carbon in the Apex chert and implications for preservation of microfossils. Astrobiology 12:160–166

Painter PC, Snyder RW, Starsinic M, Coleman MM, Kuehn DW, Davis A (1981) Concerning the application of FT-IR to the study of coal: a critical assessment of band assignments and the application of spectral analysis programs. Appl Spectrosc 35:475–485

Pasteris JD (1989) In situ analysis in geological thin-sections by laser Raman microprobe spectroscopy: a cautionary note. Appl Spectrosc 43:567–570

Qu Y, Engdhl A, Zhu S, Vajda V, McLoughlin N (2015) Ultrastructural heterogeneity of carbonaceous material in ancient cherts: investigating biosignature origin and preservation. Astrobiology 15:825–842

Rahl JM, Anderson KM, Brandon MT, Fassoulas C (2005) Raman spectroscopic carbonaceous material thermometry of low-grade metamorphic rocks: calibration and application to tectonic exhumation in Crete, Greece. Earth Planet Science Letters 240:339–354

Rasmussen B, Fletcher IR, Brocks JJ, Kilburn MR (2008) Reassessing the first appearance of eukaryotes and cyanobacteria. Nature 455:1101–1104

Robin PL, Rouxhet PG, Durand B (1977) Caracterisation des kérogènes et de leur evolution par spectroscopie infrarouge. In: Campos R, Goni J (eds) Advances in organic geochemistry 1977. Enadimsa, Madrid

Salisbury JW, Walter LS (1989) Thermal infrared (2.5-13.5 μm) spectroscopic remote sensing of igneous rock types on particulate planetary surfaces. J Geophys Res 94:9192–9202

Schopf JW, Kudryavtsev AB, Agresti DG, Czaja AD, Wdowiak TJ (2005) Raman imagery: a new approach to assess the geochemical maturity and biogenicity of permineralized Precambrian fossils. Astrobiology 5:333–371

Schopf JW, Kudryavtsev AB, Agresti DG, Wdowiak TJ, Czaja AD (2002) Laser-Raman imagery of Earth's earliest fossils. Nature 416:73–76

Sforna MC, van Zuilen MA, Philippot P (2014) Structural characterization by Raman hyperspectral mapping of organic carbon in the 3.46 billion-year-old Apex chert, Western Australia. Geochim Cosmochim Acta 124:18–33

Shen Y, Farquhar J, Masterson A, Kaufman AJ, Buick R (2009) Evaluating the role of microbial sulfate reduction in the early Archean using quadruple isotope systematics. Earth Planet Sci Lett 279:383–391

Sherwood-Lollar B, McCollom TM (2006) Biosignatures and abiotic constraints on early life. Nature 444:E18

Steemans P, Lepot K, Marshall CP, Le Hérissé A, Javaux EJ (2010) FTIR characterisation of the chemical composition of Silurian miospores (cryptospores and trilete spores) from Gotland, Sweden. Rev Palaeobot Palynol 162:577–590

Thorpe RI, Hickman AH, Davis DW, Mortensen JK, Trendall AF (1992a) U-Pb zircon geochronology of Archaean felsic units in the marble Bar region, Pilbara craton, Western Australia. Precambrian Res 56:169–189

Thorpe RI, Hickman AH, Davis DW, Mortensen JK, Trendall AF (1992b) Constraints to models for lead evolution from precise zircon U-Pb geochronology for the Marble Bar region, Pilbara Craton, Western Australia. In: Glover JE, Ho SE (eds) The Archaean: Terrains, Processes and Metallogeny. The University of Western Australia, Publication 9, Perth

Ueno Y, Isozaki Y, Yurimoto H, Maruyama S (2001) Carbon isotopic signatures of individual Archean microfossils (?) from Western Australia. Int Geol Rev 43:196–212

Ueno Y, Ono S, Rumble D, Maruyama S (2008) Quadruple Sulphur isotope analysis of ca. 3.5 Ga Dresser Formation: new evidence for microbial sulphate reduction in the early Archean. Geochim Cosmochim Acta 72:5675–5691

Ueno Y, Yamada K, Yoshida N, Maruyama S, Isozaki Y (2006) Evidence from fluid inclusions for microbial methanogenesis in the early Archaean era. Nature 440:516–519

Ueno Y, Yoshioka H, Maruyama S, Isozaki Y (2004) Carbon isotopes and petrography of kerogens in ~3.5-Ga hydrothermal silica dikes in the North Pole area, Western Australia. Geochim Cosmochim Acta 68:573–589

Van Kranendonk MJ (2006) Volcanic degassing, hydrothermal circulation and the flourishing of early life on Earth: a review of the evidence from c. 3490–3240 Ma rocks of the Pilbara Supergroup, Pilbara Craton, Western Australia. Earth-Sci Rev 74:197–240

Van Kranendonk MJ, Philippot P, Lepot K, Bodorkos S, Pirajno F (2008) Geological setting of Earth's oldest fossils in the ca. 3.5 Ga Dresser Formation, Pilbara Craton, Western Australia. Precambrian Res 167:93–124

van Zuilen MA, Chaussidon M, Rollion-Bard C, Marty B (2007) Carbonaceous cherts of the Barberton Greenstone Belt, South Africa: isotopic, chemical and structural characteristics of individual microstructures. Geochim Cosmochim Acta 71:655–669

Wacey D, Kilburn MR, Saunders M, Cliff J, Brasier MD (2011) Microfossils of sulphur-metabolizing cells in 3.4-billion-year-old rocks of Western Australia. Nat Geosci 4:698–702

Walter MR, Buick R, Dunlop JSR (1980) Stromatolites 3,400–3,500 Myr old from the North Pole area, Western Australia. Nature 284:443–445

Wang SH, Griffiths PR (1985) Resolution enhancement of diffuse reflectance i.r. spectra of coals by Fourier self-deconvolution. 1. C-H stretching and bending modes. Fuel 64:229–236

Williford KH, Ushikubo T, Schopf JW, Lepot K, Kitajima K, Valley JW (2013) Preservation and detection of microstructural and taxonomic correlations in the carbon isotopic compositions of individual Precambrian microfossils. Geochim Cosmochim Acta 104:165–182

Yanagawa H, Kobayashi K (1992) An experimental approach to chemical evolution in submarine hydrothermal systems. In: Holm NG (ed) Marine hydrothermal systems and the origin of life. Kluwer, Dordrecht

Yui TF, Huang E, Xu J (1996) Raman spectrum of carbonaceous material: a possible metamorphic grade indicator for low-grade metamorphic rocks. J Metamorph Geol 14:115–124